CHEMOMETRICS GUIDED BY SERS IMAGING: USING HOTSPOT MAPS TO IMRPOVE QUANTITATION FROM AQUEOUS ADENINE STANDARDS

Marguerite R. Butler, Dr. John B. Cooper
Department of Chemistry and Biochemistry, Old Dominion University, Norfolk, VA 23529

Abstract

Low-cost hyperspectral SERS imaging of dried droplets of silver colloidal nanoparticles and aqueous adenine was performed using a handheld 830 nm Raman spectrometer mounted on a custom-built XY translation stage. Asynchronous raster-scan data with positional timing mismatch were corrected using correction algorithms developed in LabVIEW to recover true (x,y) coordinates for every spectrum. This enabled systematic comparison of five progressive PLS models that incrementally incorporated spatial information, from blind averaging of all spectra collected across each surface (Model 1) to individual spectra inside the 9×9 pixel tile of highest average signal-to-noise (S/N) (Model 5). When applied to two independent test sets, Model 5 markedly improved inter-day robustness. While Model 1 produced highly variable results (RMSEP = 49.8 ng/mL in Test Set 1 versus 122.2 ng/mL in Test Set 2), Model 5 S/N-weighted predictions yielded nearly identical RMSEP (53.6 and 55.0 ng/mL) across both test plates and reduced the bias to nearly 0 (-3.6 ng/mL) on the more variable test plate. These results demonstrate that explicit incorporation of actual spatial positions of spectra transforms heterogeneous dried-droplet SERS into robust quantitative analysis without expensive instrumentation. This accessible strategy offers a practical route to reliable SERS quantification of aqueous biomarkers for point-of-care and other quantitative applications.

Introduction

Surface enhanced Raman spectroscopy (SERS) is a vibrational spectroscopic technique that dramatically enhances Raman scattering signals (by factors of 10^3-10^{10}) when analyte molecules are adsorbed near nanostructured noble-metal surfaces, enabling ultrasensitive, label-free molecular detection.[1] Because of its molecular specificity and high sensitivity, SERS has attracted growing interest for quantitative analysis of aqueous biomarkers.

Adenine, a purine nucleobase found in DNA and RNA, serves as a convenient model analyte for developing quantitative SERS methods (Figure 1).[2]

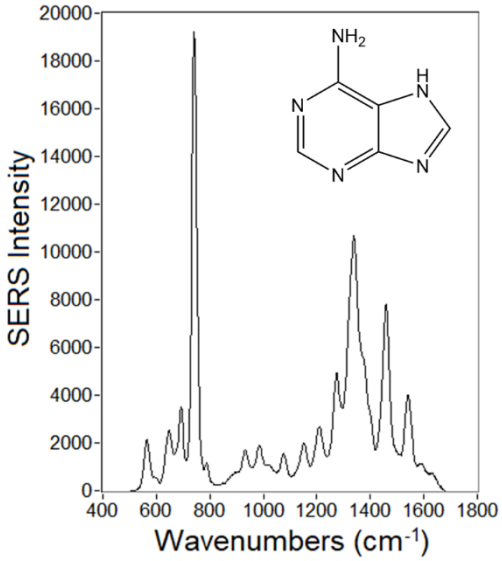

Figure 1. Chemical structure and SERS spectrum of adenine (500 ng/mL, 830 nm excitation).

However, reliable quantitation using colloidal silver nanoparticles in dried-droplet formats is hindered by well-documented challenges, including heterogeneous hotspot distribution caused by solvent evaporation and significant inter-day variability when substrates are prepared independently. In this work, mixtures of aqueous adenine and silver colloidal nanoparticles were evaporated to dryness in aluminum wells, using three independently

prepared plates to evaluate inter-day robustness.

Recent quantitative SERS imaging studies have highlighted these issues. Large-scale interlaboratory comparisons using adenine on colloidal silver and gold substrates have shown that even under controlled conditions, raw signal intensities vary substantially across instruments and laboratories.[3] Similar experiments have confirmed that substrate heterogeneity limits reproducibility, prompting the adoption of internal-standard methods to improve predictive accuracy in quantitative SERS of adenine and purine derivatives.[4]

PLS regression is a chemometric technique that models the relationship between the full spectral data (X-block) and analyte concentration (Y-block) by extracting latent variables that maximize covariance between X and Y, allowing robust predictions even in the presence of overlapping bands and matrix effects.[5]

Traditional high-resolution SERS imaging relies on confocal Raman microscopes, which provide excellent spatial detail but are expensive, time-intensive, and impractical for high-throughput or field-deployable applications. To overcome these limitations, the present study employs a low-cost handheld 830 nm Raman spectrometer mounted on a custom-built XY translation stage. Continuous raster scanning with asynchronous data acquisition is corrected using algorithms developed in LabVIEW to recover true (x,y) coordinates for every spectrum at micrometer resolution. This imaging pipeline enables systematic evaluation of five progressive PLS models that incrementally incorporate spatial information, from blind averaging of all spectra per well (Model 1) to individual spectra inside the 9×9 pixel tile corresponding to the highest average S/N (Model 5). By demonstrating that explicit use of actual spatial positions of spectra collapses inter-day variability and improves quantitative performance, this work provides a practical and accessible route to robust SERS quantitation of aqueous biomarkers without the need for expensive and time-intensive high-resolution instrumentation.

Materials and Methods

Chemicals and SERS Substrate

Adenine (≥99 %) was purchased from Sigma-Aldrich and used without further purification. Silver colloidal nanoparticles (Ag CNPs) were prepared by reduction of silver nitrate ($AgNO_3$, Sigma-Aldrich, ≥99.0 %) with hydroxylamine hydrochloride ($NH_2OH{\cdot}HCl$, Sigma) following the method of Leopold and Lendl.[6] Briefly, 300 µL of 1 M sodium hydroxide (NaOH, Fisher Chemical) was added to 90 mL of 1.6×10^{-3} M $NH_2OH{\cdot}HCl$ prepared in ultrapure Milli-Q (MQ, MilliporeSigma) water. The mixture was stirred continuously at 360 rpm while 10 mL of 1.0×10^{-2} M $AgNO_3$ was added dropwise. The suspension was stirred for an additional 45 min. The resulting colloidal suspension was stored at room temperature, protected from light.

Sample Preparation

Aqueous adenine standards were prepared at concentrations of 500, 250, 125, 62, 31, 15, and 7 ng/mL (plus a matrix blank) in ultrapure water. Each standard (500 µL) was mixed with an equal volume of AgNP suspension and vortexed for 10 s. A 20 µL aliquot of each mixture was deposited into individual 3 mm-diameter flat-bottom aluminum wells on three independently prepared plates (Datasets 1, 2, and 3). The deposited aliquots were then allowed to dry at room temperature in a chemical hood. Each of the three aluminum plates were prepared on different days. Dataset 2 served as the training set; Datasets 1 and 3 served as independent test sets to evaluate inter-day robustness.

SERS Spectral Acquisition

SERS spectra were collected using a Wasatch Photonics 830 nm Raman spectrometer mounted on a custom XY translation stage constructed in-house using Thorlabs components. Spectra were acquired continuously while the stage moved at constant velocity (integration time = 400 ms per spectrum, estimated spatial resolution of 100 µm). A full raster scan of each well produced approximately 1800 spectra. The asynchronous nature of continuous acquisition during stage motion introduced positional timing mismatch, which was later corrected in the LabVIEW image correction pipeline.

LabVIEW-Corrected Imaging Pipeline

The true spatial positions of every spectrum were recovered using software written in LabVIEW. The workflow consisted of six sequential steps: (1) continuous data acquisition, (2) S/N calculation on the 730 cm^{-1} ring-breathing mode of adenine, (3) quality filtering (S/N = 0 for saturated spectra or S/N < 10), (4) bidirectional raster correction (reversing the order of S/N values in every other row), (5) resolution enhancement (upsampling the S/N array to create ~1000 pixels per original pixel), and (6) offset correction (adjusting spectra-per-line and deleting leading spectra to apply fractional offset correction). This spatially accurate map enabled explicit 9×9 pixel hotspot-tile selection and pixel-by-pixel PLS predictions. The full S/N maps of every aluminum well in the training set are shown in Figure 2.

Spectral Preprocessing

All spectra were preprocessed identically: 5-point Savitzky–Golay smoothing (2nd-order polynomial), truncation to spectral region 503.40-1679.82 cm^{-1}, and 2-point baseline correction. Signal-to-noise (S/N) ratios calculated from the 730 cm^{-1} adenine ring-breathing mode were used for hotspot selection.

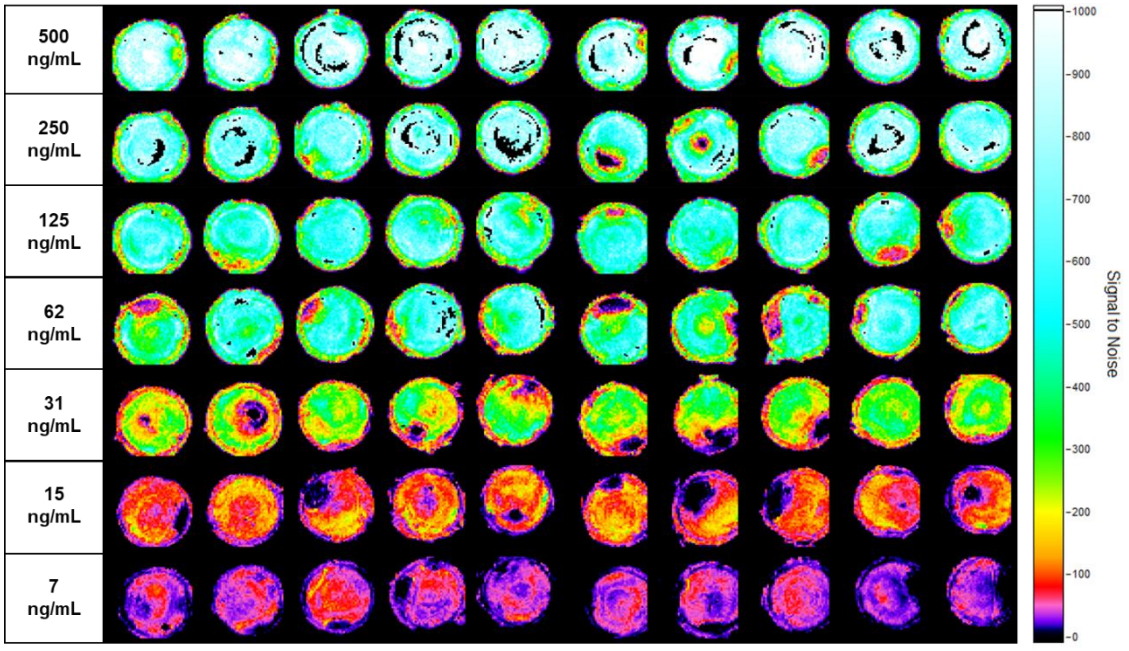

Figure 2. S/N maps of every aluminum well in the training set (each row corresponds to one adenine concentration from 500 to 7 ng/mL). The S/N was calculated on the 730 cm^{-1} adenine ring-breathing mode. Saturated spectra and spectra with S/N < 10 are assigned S/N = 0 (black pixels).

Partial Least-Squares (PLS) Regression

PLS models were built using in-house LabVIEW software, with Dataset 2 as the training set and 5-fold cross-validation. Mean-centering was applied to both X (spectra) and Y (concentration) blocks. Optimal numbers of latent variables (LVs) were selected by minimizing the root-mean-square error of cross-validation (RMSECV). Five progressive models were constructed that incrementally incorporated spatial information from the corrected imaging maps (see *LabVIEW-Corrected Imaging Pipeline*). For each model, the identical spectral selection and averaging strategy used during training was applied to the independent test sets so that the conditions matched exactly. Model 1 used the average of all spectra per well; Models 2 and 3 used the top 18 (≈1 %) highest-S/N spectra (averaged or individual); Models 4 and 5 used the spectra inside the 9×9 pixel tile of highest average S/N (averaged or individual). In Model 5, S/N-weighted averaging of the test set concentration predictions was performed.

Results

The five PLS models were constructed on Dataset 2 (training set) with 5-fold cross-validation, using the identical spectral selection and averaging strategy for both training and independent test sets (Datasets 1 and 3). Optimal numbers of latent variables (LVs) were chosen by minimizing the root-mean-square error of cross-validation (RMSECV; Figure 3). Models 1 and 2 (global or simple S/N averages) required only 6 LVs, while Models 3-5, which preserve individual spectra or spatially resolved tiles, required 7-12 LVs (Tables 1 and 2). This modest increase in model complexity is expected in PLS when extraneous low-enhancement spectra are removed and spatial information is considered, allowing the latent-variable decomposition to capture more chemically relevant variance.

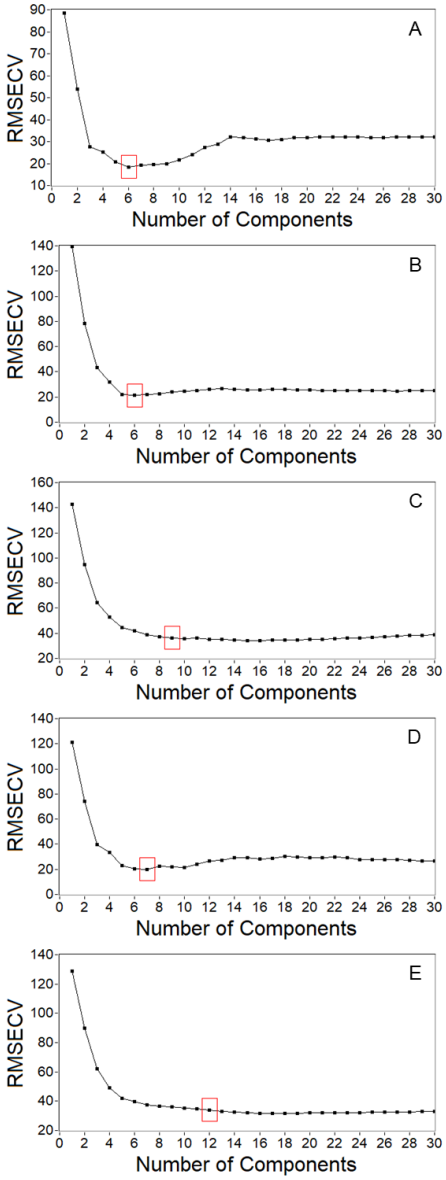

Figure 3. Root-mean-square error of 5-fold cross-validation (RMSECV) versus number of latent variables retained for each PLS model: (A) Model 1, (B) Model 2, (C) Model 3, (D) Model 4, and (E) Model 5. Optimal numbers of latent variables selected for the final models are highlighted by red boxes.

Performance metrics on the two independent test plates are summarized in Table 1 and Table 2.[1] In Test Set 1 (Dataset 1, Table 1), progression from blind

[1]In Tables 1 and 2, bias is defined as the mean difference between the predicted and actual concentrations.

averaging (Model 1: RMSEP = 49.8 ng/mL, R^2 = 0.915, slope = 0.967) to selection of the top 18 highest-S/N spectra (Model 3) reduced RMSEP to approximately 40.8 ng/mL. Explicit spatial hotspot selection via the 9×9 pixel tile (Models 4 and 5) produced slightly higher absolute error (Model 5 S/N-weighted: RMSEP = 53.6 ng/mL) yet restored a nearly perfect slope of 0.999.

Test Set 2 (Dataset 3, Table 2) demonstrated the power of incorporating true spatial positions in the PLS models. Blind averaging (Model 1) failed dramatically (RMSEP = 122.2 ng/mL, slope = 0.413, bias = –71.6 ng/mL), exposing severe inter-experiment variability. Progressive spatial incorporation steadily recovered performance; Model 5 (individual spectra inside the highest-average-S/N 9×9 tile) with S/N-weighted averaging of the per-pixel predictions delivered the strongest result (RMSEP = 55.0 ng/mL, R^2 = 0.939, slope = 0.726, bias = –3.6 ng/mL). Critically, Model 5 S/N-weighted predictions showed nearly identical RMSEP across the two test plates (53.6 vs. 55.0 ng/mL), demonstrating markedly improved robustness to inter-day experimental variability.

Table 1. PLS model performance metrics for Test Set 1.

Test Set 1					
	PLS Model 1	**PLS Model 2**	**PLS Model 3** (individual top-18 spectra, averaged predictions)	**PLS Model 4**	**PLS Model 5** (individual 9x9-tile spectra, S/N weighted predictions)
# LVs retained	6	6	9	7	12
Slope	0.967	1.082	1.082	0.838	0.999
Intercept	12.20	5.07	-9.71	21.03	13.46
R^2	0.915	0.964	0.958	0.884	0.911
RMSEP	49.8	40.8	40.0	57.2	53.6
Bias	7.6	16.7	1.9	-1.9	13.4

Table 2. PLS model performance metrics for Test Set 2.

Test Set 2					
	PLS Model 1	**PLS Model 2**	**PLS Model 3** (individual top-18 spectra, averaged predictions)	**PLS Model 4**	**PLS Model 5** (individual 9x9-tile spectra, S/N weighted predictions)
# LVs retained	6	6	9	7	12
Slope	0.413	0.738	0.668	0.712	0.726
Intercept	11.42	7.20	5.80	-2.44	35.08
R^2	0.942	0.903	0.930	0.934	0.939
RMSEP	122.2	66.3	75.3	71.8	55.0
Bias	-71.6	-29.8	-41.2	-43.2	-3.6

Regression vectors for all five PLS models exhibited a prominent feature at the adenine ring-breathing mode in the 730 cm^{-1} region (Figure 4). As spatial information was progressively incorporated through hotspot selection, the regression vectors showed changes in relative peak intensities, consistent with greater focus on chemically meaningful features. Predicted-versus-actual plots (Figure 5) further illustrate this trend, where Model 1 shows excellent agreement on Test Set 1 but collapses on Test Set 2 (Figure 5A), while Model 5 (S/N-weighted) aligns the predicted concentrations of both independent plates closely with each other (Figure 5E). Pixel-by-pixel application of Model 5 across each well, made possible only by the LabVIEW-spatial correction pipeline, generated predicted-concentration maps for all test-set wells (Figure 6 and Figure 7).

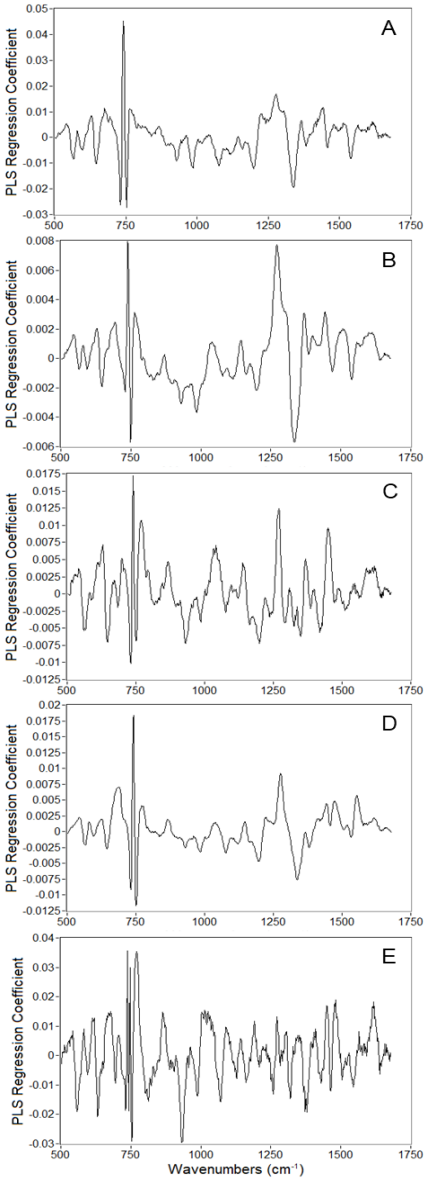

Figure 4. Regression vectors for (A) Model 1, (B) Model 2, (C) Model 3, (D) Model 4, and (E) Model 5.

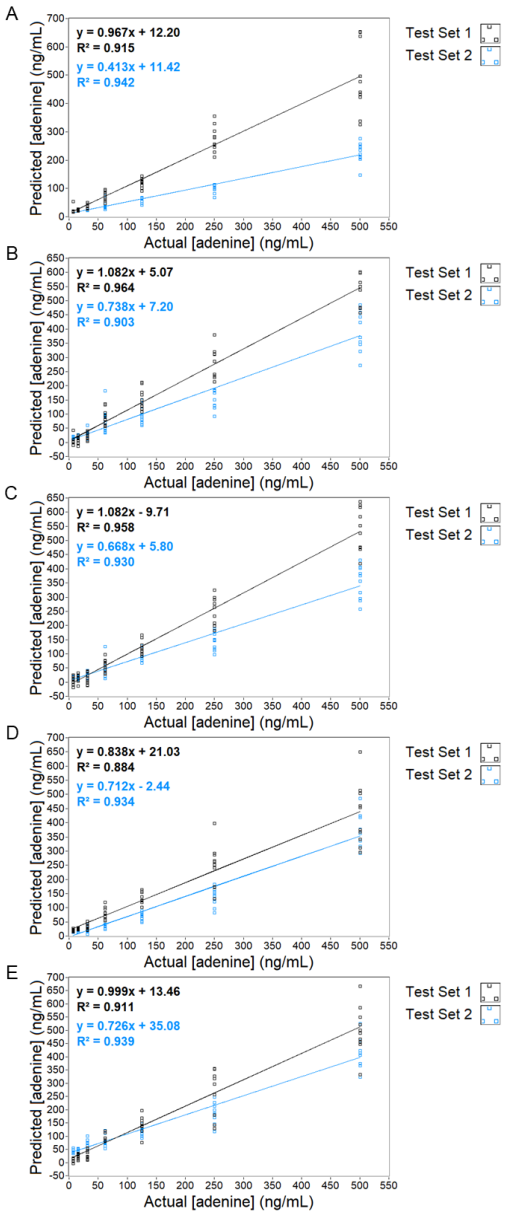

Figure 5. Predicted-versus-actual concentration plots for Models 1-5 (A-E). Test Set 1 (black) and Test Set 2 (blue) are overlaid on each panel along with the linear regression line and corresponding R^2 value.

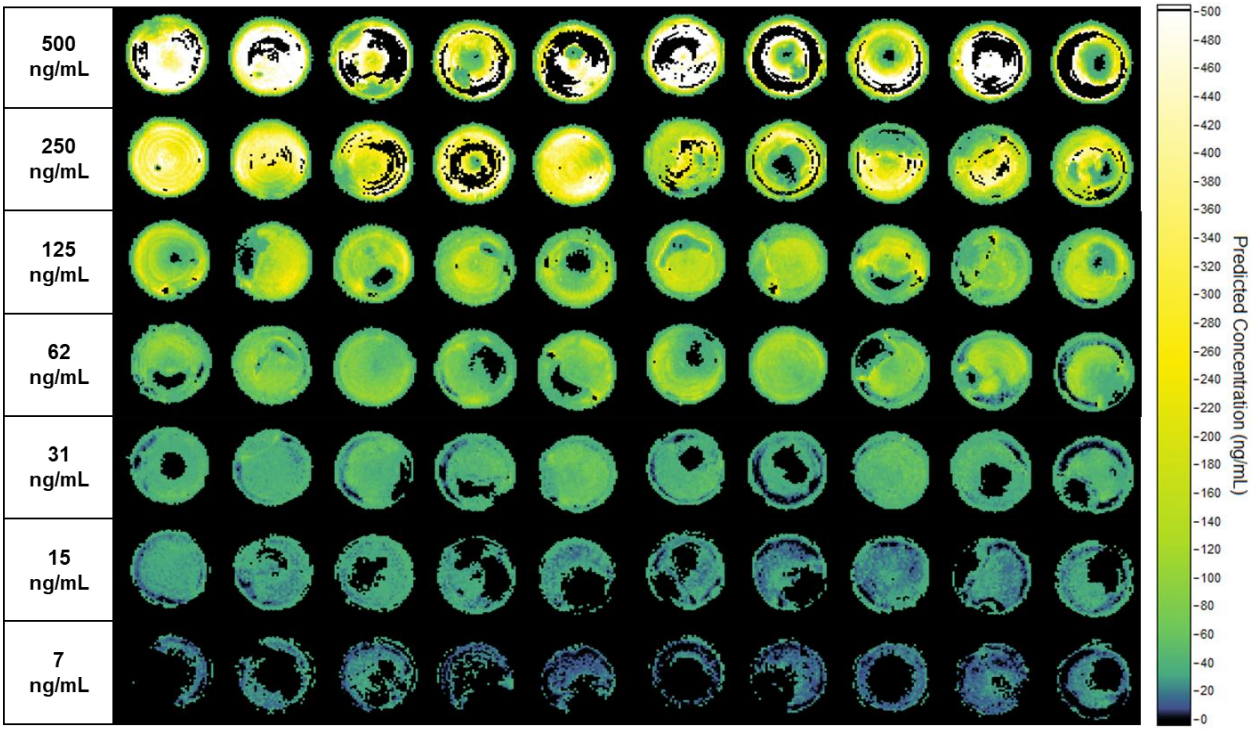

Figure 6. Predicted-concentration maps for all wells in Test Set 1 generated by pixel-by-pixel application of Model 5. Black pixels correspond to saturated spectra or spectra with S/N < 10.

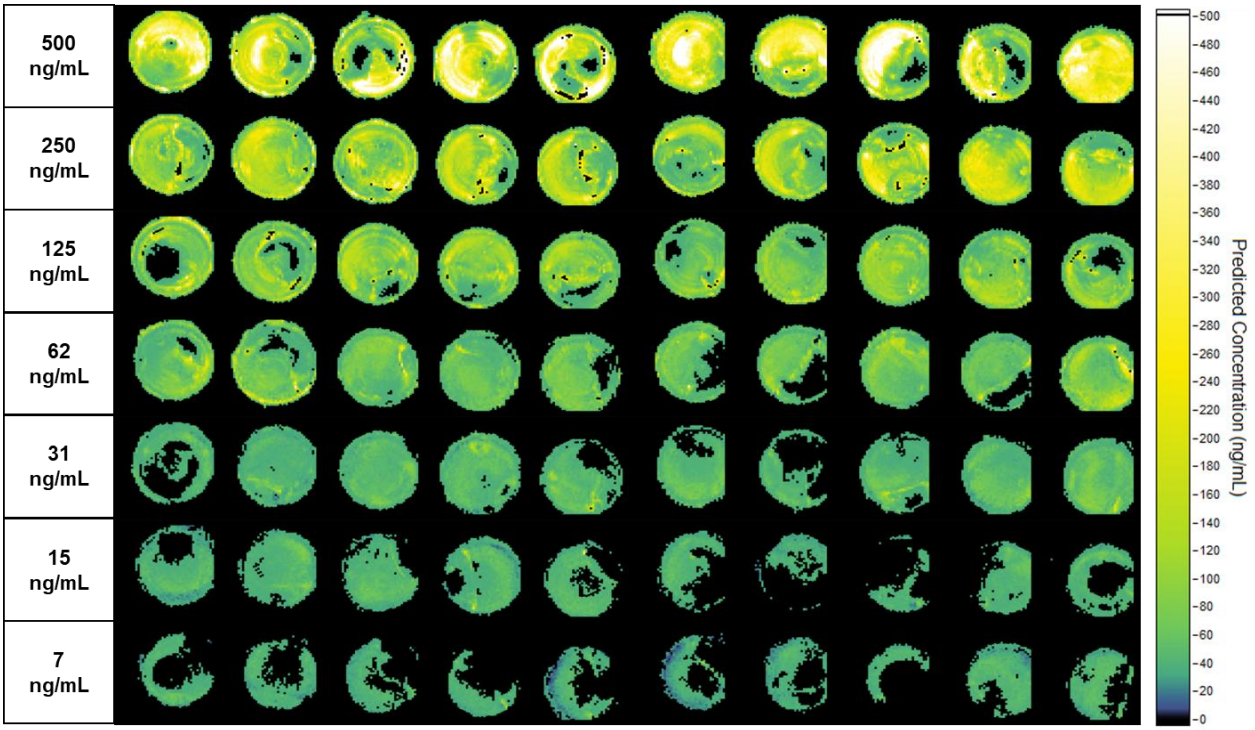

Figure 7. Predicted-concentration maps for all wells in Test Set 2 generated by pixel-by-pixel application of Model 5. Black pixels correspond to saturated spectra or spectra with S/N < 10.

Discussion

The progressive PLS models demonstrate that incorporating the actual spatial positions of spectra substantially improves quantitative performance and inter-day robustness in heterogeneous dried-droplet SERS. By moving from global blind averaging (Model 1) to explicit 9×9 hotspot-tile selection with S/N-weighted predictions (Model 5), the approach systematically mitigates the impact of low-enhancement regions that dominate variability across independently prepared plates.

In Test Set 2 (Table 2), blind averaging produced extremely high RMSEP (122.2 ng/mL) and severe bias (−71.6 ng/mL), reflecting large inter-day differences in nanoparticle aggregation and enhancement. Once spatial information was considered, performance recovered dramatically: Model 5 S/N-weighted predictions reduced RMSEP to 55.0 ng/mL and bias to −3.6 ng/mL, while restoring a slope of 0.726. Most importantly, RMSEP values for Model 5 became nearly identical across the two test plates (53.6 ng/mL in Test Set 1 versus 55.0 ng/mL in Test Set 2), confirming that the combination of hotspot-tile selection and S/N-weighted averaging effectively collapses inter-day variability.

The predicted concentration maps for all wells in both test sets (Figures 6 and 7), generated by pixel-by-pixel application of Model 5, exhibit a clear concentration-dependent gradient, with higher predicted values (yellow/white) comprising the majority of the aluminum wells containing higher adenine concentrations. These maps, produced directly from the LabVIEW-corrected imaging pipeline, provide visual evidence that respecting the true (x,y) positions of spectra converts heterogeneous data into reliable quantitative output.

Remaining limitations are modest. In the less variable Test Set 1, Model 5 shows slightly higher absolute RMSEP than the non-spatial Model 3, indicating a small trade-off between spatial coherence and raw per-spectrum precision. In addition, the slope in Test Set 2 remains imperfect (0.726), suggesting residual nonlinearity at low concentrations that future refinements (adaptive tile sizes or ensemble modeling across multiple hotspots) could address.

Overall, the low-cost XY-stage system combined with simple LabVIEW correction algorithms offers a practical route to quantitative SERS mapping without expensive high-resolution instrumentation. The results highlight that explicit incorporation of spatial information, rather than blind averaging, is a powerful and accessible strategy for improving PLS regression in heterogeneous SERS substrates.

Conclusion

Spatial incorporation of the actual positions of spectra, achieved through a low-cost XY-stage imaging pipeline with carefully designed spatial correction algorithms, substantially improves quantitative PLS regression in heterogeneous dried-droplet SERS. By progressing from global blind averaging to 9×9 hotspot-tile selection with S/N-weighted averaging of predictions (Model 5), inter-day variability is collapsed, and prediction bias is reduced by an order of magnitude. The resulting predicted-concentration maps provide direct visual confirmation that high-S/N regions dominate the signal, offering a practical and accessible route to reliable adenine quantification. Future work will explore adaptive tile sizes, ensemble modeling across multiple hotspots, and extension to other analytes.

Acknowledgements

The authors gratefully acknowledge support from the Virginia Space Grant Consortium (VSGC) Graduate Research Fellowship.

References

(1) Schlücker, S. Surface-Enhanced Raman Spectroscopy: Concepts and Chemical Applications. *Angewandte Chemie International Edition* **2014**, *53* (19), 4756-4795. DOI: 10.1002/anie.201205748.

(2) Sloan-Dennison, S.; Wallace, G. Q.; Hassanain, W. A.; Laing, S.; Faulds, K.; Graham, D. Advancing SERS as a quantitative technique: challenges, considerations, and correlative approaches to aid validation. *Nano Convergence* **2024**, *11* (1), 33. DOI: 10.1186/s40580-024-00443-4.

(3) Fornasaro, S.; Alsamad, F.; Baia, M.; Batista de Carvalho, L. A. E.; Beleites, C.; Byrne, H. J.; Chiadò, A.; Chis, M.; Chisanga, M.; Daniel, A.; et al. Surface Enhanced Raman Spectroscopy for Quantitative Analysis: Results of a Large-Scale European Multi-Instrument Interlaboratory Study. *Analytical Chemistry* **2020**, *92* (5), 4053-4064. DOI: 10.1021/acs.analchem.9b05658.

(4) Cheng, H. W.; Tsai, H. M.; Wang, Y. L. Exploiting Purine as an Internal Standard for SERS Quantification of Purine Derivative Molecules Released by Bacteria. *Anal Chem* **2023**, *95* (46), 16967-16975. DOI: 10.1021/acs.analchem.3c03259.

(5) Goodacre, R.; Graham, D.; Faulds, K. Recent developments in quantitative SERS: Moving towards absolute quantification. *TrAC Trends in Analytical Chemistry* **2018**, *102*, 359-368. DOI: 10.1016/j.trac.2018.03.005.

(6) Leopold, N.; Lendl, B. A New Method for Fast Preparation of Highly Surface-Enhanced Raman Scattering (SERS) Active Silver Colloids at Room Temperature by Reduction of Silver Nitrate with Hydroxylamine Hydrochloride. *The Journal of Physical Chemistry B* **2003**, *107* (24), 5723-5727. DOI: 10.1021/jp027460u.